Stiffness of Soil–Geosynthetic Composite under Small Displacements: I. Model Development

Jorge G. Zornberg, M.ASCE[1]; Gholam H. Roodi, M.ASCE[2]; and Ranjiv Gupta, M.ASCE[3]

Abstract: While significant emphasis has been placed on the quantification of soil–geosynthetic properties under failure conditions, studies of properties that are suitable for characterizing this interaction under serviceability conditions have been limited. Also, most geosynthetic properties are currently defined in isolation rather than under the confinement of soil. The purpose of this study is to develop a soil–geosynthetic interaction framework that, with a single and repeatable parameter, can capture the stiffness of a soil–geosynthetic composite under small displacements. The soil–geosynthetic interaction model developed in this study involves well-established force equilibrium differential equations. However, the constitutive relationships and boundary conditions were specifically selected so that the model results in a closed-form analytical solution. Since the analytical solution involves a single parameter, its use may be particularly suitable for specifications and the design of structures such as stabilized roadways. This parameter, referred to as the *stiffness of the soil–geosynthetic composite*, or K_{SGC}, captures both the tensile characteristics of the geosynthetic and the shear behavior of the soil–geosynthetic interface. Experimental procedures to quantify K_{SGC} were developed as part of this study. The results of a pilot experimental program, conducted using tailor-made soil–geosynthetic interaction equipment, are presented in the paper. These results confirm the suitability of the assumptions and outcomes of the model. A companion paper provides the results of a comprehensive experimental program with particular emphasis on the evaluation of the repeatability of the results and on the sensitivity of the assumptions and outcomes of the model to variables that impact K_{SGC}.
DOI: 10.1061/(ASCE)GT.1943-5606.0001768.

Author keywords: Stiffness; Soil–geosynthetic interaction; Soil reinforcement; Extensible reinforcements; Geosynthetics; Pullout test; Stabilization.

Introduction

Geosynthetic inclusions have been extensively used to enhance the mechanical response in two groups of geotechnical systems: (1) geotechnical structures that are designed using criteria associated with the structure's limit state (e.g., reinforced soil walls, reinforced steep slopes) and (2) geotechnical structures that are designed using deformability or serviceability criteria (e.g., stabilized bases and subgrades in roadway systems). In the case of reinforced walls and steep slopes, the internal stability analysis requires that geosynthetics be selected to account for the development of shear surfaces within the reinforced soil mass. Tensile forces (and strains) develop along the geosynthetics, with a maximum value occurring at the locus of the potential failure surface (Allen et al. 1992; Zornberg et al. 1997; Zornberg and Arriaga 2003). On the other hand, geosynthetics have also been used in roadway applications, either by placing the geosynthetic within the unbound base layer or at the subbase–subgrade interface to improve the performance of a roadway under both traffic and environmental loads (e.g., Al-Qadi et al. 2008; Giroud and Han 2004a, b; Roodi and Zornberg 2012; Zornberg et al. 2012a, c). Specifically, geosynthetics have been used in roadway base layers to minimize the lateral spreading of granular particles (and the consequent degradation of the base layer stiffness) through lateral restraint mechanisms. While failure criteria govern the design of geosynthetic-reinforced retaining structures, deformability criteria under comparatively small displacements govern the performance of geosynthetic-stabilized roadways. Additional examples of geosynthetic systems designed using deformability or serviceability criteria include geosynthetic-stabilized rail subballast (e.g., Biabani and Indraratna 2015), geosynthetic-encased stone columns (e.g., Gu et al. 2016), and geosynthetic-reinforced airport pavements (e.g., Abdesssemed et al. 2015). Recent studies have focused not only on the mechanical but also on additional sustainability benefits resulting from the use of geosynthetics in combination with recycled aggregates and industrial byproducts (e.g., Han and Thakur 2015; Hanumasagar et al. 2014; Xiao et al. 2015; Pando et al. 2014).

Because the initial use in the geotechnical practice of geosynthetics involved reinforcement of retaining structures, the methodologies and models developed for the analysis of geosynthetics in geotechnical structures have traditionally relied on the quantification of properties related to limit conditions (e.g., tensile strength, pullout resistance). However, the quantification of stiffness properties of a soil–geosynthetic composite is key to understanding the behavior of other structures such as geosynthetic-stabilized roadway systems. In the absence of properties suitable for characterizing soil–geosynthetic interfaces under small displacements, designers have typically relied on the mechanical properties of geosynthetics in isolation (e.g., ultimate tensile strength, tensile stiffness) to achieve a target performance level. Accordingly, studies have aimed at establishing correlations between geosynthetic index properties and their performance in field applications. In the case of geogrids,

[1]Professor, Dept. of Civil, Architectural, and Environmental Engineering, Univ. of Texas at Austin, Austin, TX 78712 (corresponding author). E-mail: zornberg@mail.utexas.edu

[2]Postdoctoral Fellow, Dept. of Civil, Architectural, and Environmental Engineering, Univ. of Texas at Austin, Austin, TX 78712. E-mail: hroodi@utexas.edu

[3]Project Engineer, Geosyntec Consultants, Phoenix, AZ 85028.

Note. This manuscript was submitted on October 25, 2016; approved on April 17, 2017; published online on July 29, 2017. Discussion period open until December 29, 2017; separate discussions must be submitted for individual papers. This paper is part of the ***Journal of Geotechnical and Geoenvironmental Engineering***, © ASCE, ISSN 1090-0241.

index properties have included the geogrid rib strength, junction strength, wide-width tensile strength, tensile modulus, unit tension at 2 and 5%, and flexural rigidity (e.g., Chen and Abu-Farsakh 2012; Christopher et al. 2008; Cuelho and Perkins 2009; Perkins et al. 2004). However, most of these properties involve the behavior of geosynthetics in isolation rather than a confined interaction between soil and geosynthetic.

The purpose of this study is to develop a soil–geosynthetic interaction framework that, with a single and repeatable parameter, captures the stiffness of a soil-geosynthetic composite under confined conditions and for small displacements. This paper details the assumptions, formulations, development, and solution of a model that provides the framework for such a stiffness parameter. This model is referred to as the soil-geosynthetic composite (SGC) model. The paper also reports on the results obtained from a pilot large-scale soil–geosynthetic interaction test, conducted to evaluate the basic assumptions and predictions of the model. A companion paper (Roodi and Zornberg 2017) provides the results of a comprehensive experimental program, with particular emphasis on the evaluation of the repeatability of the experimental results and of the sensitivity of the assumptions and outcomes of the model to variables that impact the stiffness of the soil-geosynthetic composite (K_{SGC}).

Background on Analytical Models

The analytical studies previously conducted to evaluate the behavior of geosynthetic-reinforced systems can be grouped according to two main approaches. The initial approach, introduced in the 1970s, assumed that the reinforced soil mass behaves as a homogenized material that presents an equivalent cohesion (Yang 1972) or an anisotropic response based on Mohr-Coulomb theory (Schlosser and Long 1973). Although this approach resulted in reinforced soil models with simple solutions, these models provided a limited representation of the interface between soil and geosynthetics. In particular, these approaches could not distinguish between the stresses and strains in the soil and those in the geosynthetic inclusions. The second approach, which has been used since the 1990s, involves representing the soil and geosynthetic as two discrete materials. This approach requires characterization of the soil, the geosynthetic, and the interface between soil and the geosynthetic inclusions.

Accordingly, the use of a discrete model requires that suitable constitutive relationships be defined for (1) the backfill soil, (2) the geosynthetic, and (3) the soil–geosynthetic interface. Simple models have been used for structures incorporating inextensible reinforcements because the interaction could be interpreted as movement of the entire reinforcement without elongation. However, more complex models are needed for extensible reinforcements because the interaction in this case involves both relative soil–geosynthetic displacements and elongation of the geosynthetic. This complex interaction results in the progressive development of tension in the extensible reinforcement, with mobilization of interface shear along its length.

Modeling of soil–geosynthetic interaction can account for the local mechanisms and actual geometry of the geosynthetic. The two main types of geosynthetic inclusions involve (1) geogrids, which involve a regular network of members (e.g., longitudinal and transverse members) that form apertures that interlock with the surrounding soil media, and (2) sheet reinforcements, which involve planar surfaces without openings. The presence of transverse members in geogrids has been reported to mobilize bearing resistance mechanisms, whereas the main resistance mechanism in sheet reinforcements involves shear that develops at the geosynthetic surface. Hence, while modeling sheet reinforcements has involved only the frictional resistance at the interface, modeling of geogrids has also accounted for bearing resistance of the soil (e.g., Wilson-Fahmy and Koerner 1993). Furthermore, the advent of geogrids with triangular-shaped apertures requires proper accounting of the geosynthetic geometry (Archer and Wayne 2012; Swan and Yuan 2013a, b). Alternatively, to preserve the simplicity of the analytical solutions for geogrids, an equivalent interface shear has often been adopted to represent the combined effects of (1) frictional resistance acting on the top and bottom plane areas of longitudinal and transverse members and (2) bearing resistance acting against transverse members.

A number of studies have been reported considering separate models for soil bearing resistance and geogrid transverse members. The ultimate soil bearing resistance has been estimated using approaches suggested by Peterson and Anderson (1980) and Jewell et al. (1984), which were developed on the basis of the general failure mechanism for shallow footings (Terzaghi 1943) and punching failure for deep foundations (Vesic 1963). These equations were later recognized as upper and lower bounds for the soil bearing resistance in pullout tests (Jewell 1996; Palmeira and Milligan 1989). An additional formulation was proposed by Matsui et al. (1996) based on Prandtl's failure mechanism. The predictions obtained using this formulation lay within the upper and lower limits. The soil bearing stress–displacement response has often been modeled using hyperbolic functions (Bergado and Chai 1994; Wilson-Fahmy and Koerner 1993). Transverse ribs of geogrids have been modeled using a number of approaches, including (1) a flexible-rib model for transverse ribs that have negligible flexural rigidity, (2) a stiff-rib model for relatively rigid transverse members, and (3) a beam model for transverse members responding with some flexural rigidity (Wilson-Fahmy and Koerner 1993). However, the rigorous formulations have only been solved using numerical approaches such as finite elements and finite differences (e.g., Sieira et al. 2009; Wilson-Fahmy and Koerner 1993).

Comparatively simple constitutional relationships adopted in previous studies for sheet reinforcements have also been adopted for geogrids by assuming an equivalent interface shear strength. In these studies, the resulting soil–geosynthetic interaction formulation will depend on the models selected for (1) the geosynthetic and (2) the soil–geosynthetic interface. The geosynthetic constitutive model describes its unit tension versus strain response and can be obtained by tensile testing of the geosynthetic in isolation. Although the unit tension–strain response of geosynthetics is inherently nonlinear, a linear response has often been adopted (e.g., Alobaidi et al. 1997; Gurung and Iwao 1999; Juran and Chen 1988; Sobhi and Wu 1996; Yuan 2011). However, nonlinear functions have also been used, including polynomial functions (Bergado and Chai 1994; Wilson-Fahmy and Koerner 1993) and hyperbolic functions (Perkins and Cuelho 1999; Sieira et al. 2009; Weerasekara and Wijewickreme 2010).

Interface constitutive relationships relate the shear stress mobilized at the soil–geosynthetic interface to the relative displacements that are mobilized between these two materials. Experimental data have been obtained to determine this relationship using interface direct shear tests in which pure shear is induced between a soil layer and a geosynthetic specimen. Models adopted in previous studies to describe the interface interaction include linear elastic (Yuan 2011), linear elastic–perfectly plastic (Juran and Chen 1988; Bergado and Chai 1994), rigid–perfectly plastic (Sobhi and Wu 1996), bilinear and hyperbolic models (Alobaidi et al. 1997; Gurung and Iwao 1999; Sieira et al. 2009; Wilson-Fahmy and Koerner 1993), and more complex nonlinear multiphase models such as elastoplastic strain hardening and softening models (Juran and Chen 1988; Perkins and Cuelho 1999), as well as linear prepeak followed by nonlinear postpeak response (Weerasekara and Wijewickreme 2010).

The use of different constitutive models and boundary conditions has led to a wide range of formulations to solve the differential equations that result after considering force equilibrium in a soil–geosynthetic system. However, owing to the complexity of these formulations, the reported solutions have often involved the use of numerical techniques, including finite elements and finite differences (e.g., Alobaidi et al. 1997; Bergado and Chai 1994; Weerasekara and Wijewickreme 2010; Wilson-Fahmy and Koerner 1993). Even though a limited number of closed-form solutions have been reported in the literature (e.g., Juran and Chen 1988; Sobhi and Wu 1996), these solutions have focused on predicting the pullout force versus displacement response and have resulted in multiparameter solutions rather than a single parameter that could characterize the stiffness of a soil-geosynthetic composite. Consequently, an important goal of this study was to develop a closed-form analytical solution that involves a single, repeatable parameter that could characterize the initial stiffness of a soil-geosynthetic composite. Additional important objectives of this study were to develop the experimental approach to quantify such a soil–geosynthetic interaction parameter, as well as to validate the constitutive models that led to its determination.

Development of the SGC Model

As part of this study, a significant number of constitutive relationships and boundary conditions were evaluated to solve the differential equation governing the soil–geosynthetic interaction. Ultimately, the relationships, boundary conditions, and formulations finally adopted in this study were those that led to a closed-form solution that involves a single parameter that captures the stiffness of a soil-geosynthetic composite under small displacements. This section presents the adopted analytical framework. As will be discussed subsequently in the paper, suitable experimental procedures could be readily implemented to determine all constitutive parameters in the model.

Adopted Constitutive Relationships

Specific constitutive relationships for both the geosynthetic and the soil–geosynthetic interface had to be adopted in order to develop the model proposed in this study. The constitutive law adopted for the geosynthetic relates its unit tension (T) to the corresponding tensile strain (ε). Specifically, a linear relationship with a slope referred to as the confined geosynthetic stiffness or J_c was assumed to represent the geosynthetic unit tension (T) versus tensile strain (ε) [Fig. 1(a)]:

$$T = J_c \cdot \varepsilon \tag{1}$$

The unit tension (T), which is the applied force per unit width of the geosynthetic, has been commonly used to represent the load in geosynthetics. The confined stiffness J_c also corresponds to $E \cdot t$, where E is the elastic modulus of the geosynthetic and t is its thickness.

It should be noted that J_c was used in this study for the confined stiffness, while J was used to represent its in-isolation stiffness. The effect of confinement on the unit tension–strain response of geosynthetics has been evaluated in other studies (e.g., Christopher et al. 1986; El-Fermaoui and Nowatzki 1982; Kokkalis and Papacharisis 1989; Leshchinsky and Field 1987; McGown et al. 1982; Mendes et al. 2007; Palmeira et al. 1996; Siel et al. 1987; Wu 1991; Zornberg et al. 1998a). The effect of confinement has been reported to be particularly relevant for nonwoven geotextiles (Palmeira 2009) owing to (1) increased interlocking and friction among geotextile fibers and (2) intrusion of soil particles into geotextile voids (impregnation), which reduces the space available for fiber stretching. In addition, the confinement of soil also minimizes geosynthetic necking during the development of tension, which may affect the geosynthetic stiffness.

The linear unit tension–strain response adopted in this study has often been adopted in previous studies because it is deemed to be particularly suitable for confined conditions under small displacements. It has been reported that nonlinear modeling of the geosynthetic response becomes necessary only when approaching tensile failure (Perkins and Cuelho 1999).

A constitutive relationship for the soil–geosynthetic interface, which relates the shear stress (τ) to the relative displacement between soil and geosynthetic (u), was also adopted to formulate the SGC model. Specifically, a rigid–perfectly plastic response was assumed in this study to relate the interface shear stress to displacement. Adopting this assumption led to simplification of the governing differential equation for soil–geosynthetic interaction and, consequently, to a closed-form analytical solution. The rigid–perfectly plastic relationship for the soil–geosynthetic interface implies that the interface shear was not assumed to change with displacement. A yield shear stress, referred to herein as τ_y [Fig. 1(b)], develops for nonzero displacements as follows:

$$\tau(u) = 0 \quad \text{for } u = 0 \tag{2a}$$

$$\tau(u) = \tau_y \quad \text{for } u > 0 \tag{2b}$$

As stated previously, the constitutive relationships described in this section were adopted because they lead to a closed-form solution that can be verified experimentally. In addition, since the displacements within the confined soil are significantly smaller than those in the geosynthetic, the relative displacement between soil and geosynthetic was assumed to be equal to the total displacement in the geosynthetic. This is deemed acceptable for a testing setup where the geosynthetic is pulled out of the soil.

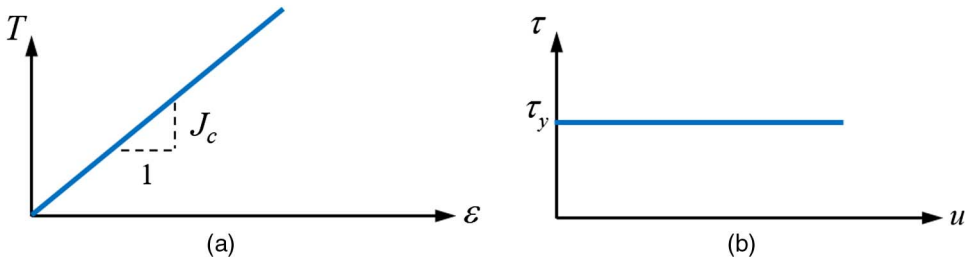

Fig. 1. Constitutive relationships adopted in this study: (a) unit tension-strain relationship for confined geosynthetics; (b) soil–geosynthetic interface shear

J. Geotech. Geoenviron. Eng., 2017, 143(10): 04017075

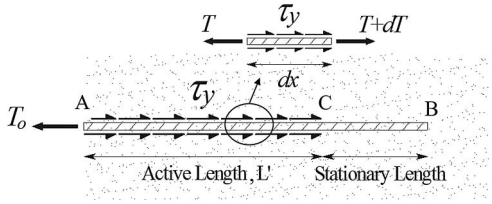

Fig. 2. Boundary conditions adopted in formulation

Formulation

The governing differential equation for soil–geosynthetic interaction results from considering the local force equilibrium of a differential control segment of the geosynthetic (Fig. 2). The use of nonlinear constitutive relationships for any of the materials could lead to nonlinear differential equations that do not result in closed-form solutions, requiring numerical methods instead.

Considering the force equilibrium of a differential segment of confined geosynthetics (Fig. 2), the differential equation governing soil–geosynthetic interaction can be represented by

$$\frac{dT}{dx} = -2\tau \tag{3}$$

where dx = length of a differential segment of the geosynthetic; T = geosynthetic unit tension; and τ = interface shear stress between soil and geosynthetic.

Consistent with the interface constitutive relationship assumed in this study, the soil–geosynthetic interface shear is constant (i.e., $\tau = \tau_y$) along the segment of geosynthetic length, referred to as the geosynthetic active length (L'), where shear has been mobilized (Fig. 2). Therefore, the soil–geosynthetic interface shear has been assumed not to be a function of displacement. Incorporating Eqs. (1) and (2) into Eq. (3) results in

$$\frac{d(J_c\varepsilon)}{dx} = -2\tau_y \tag{4}$$

The geosynthetic tensile strain (ε) at a location x can be expressed as the derivative of the geosynthetic displacement (u) at that location. In addition, since J_c is considered constant for a given normal pressure and under small displacements, Eq. (4) can be rewritten as follows:

$$-J_c\frac{d^2u}{dx^2} = -2\tau_y \tag{5}$$

Eq. (5) can be simplified to yield

$$\frac{d^2u}{dx^2} = \frac{2\tau_y}{J_c} \tag{6}$$

Integrating twice the differential Eq. (6) results in a solution for u, as follows:

$$u = \frac{\tau_y}{J_c}x^2 + c_1x + c_2 \tag{7}$$

where c_1 and c_2 are constants of integration.

Boundary Conditions and Solution

Determination of the constants c_1 and c_2 in Eq. (7) requires considering two boundary conditions. As illustrated in Fig. 2, under a given confining pressure and for a given applied tension, shear has been mobilized only along a portion of the geosynthetic length [active length (L')]. As the frontal load increases, the mobilized (active) length of the geosynthetic will also increase. This progressive mobilization of the interface shear resistance continues until shear is mobilized along the entire length of the geosynthetic (or until the geosynthetic breaks in tension, if this condition occurs first).

Solutions reported in the literature have typically used two force (or strain) boundary conditions at the two ends of the geosynthetic to solve the governing differential equation (e.g., Gurung and Iwao 1999). Specifically, boundary conditions typically reported in the literature include (1) $T = T_0$ (or $\varepsilon = \varepsilon_0$) at $x = 0$ (Point A in Fig. 2) and (2) $T = 0$ (or $\varepsilon = 0$) at $x = L$ (Point B in Fig. 2). Although these boundary conditions may be suitable, particularly for rigid reinforcements, their use does not lead to closed-form solutions. As an alternative, the approach considered in this study results from recognizing that a portion of the length of the extensible reinforcement (Stationary Length BC in Fig. 2) had not been mobilized.

Accordingly, a force boundary condition can be assumed at the loading front of the geosynthetic (Point A in Fig. 2), while a displacement boundary condition can be assumed at the end of the active length of the geosynthetic, where the stationary portion of the geosynthetic begins (Point C in Fig. 2). This approach involves adopting a moving boundary condition to solve the differential equation since the active length of the geosynthetic, L', increases with increasing frontal tension. Therefore, the boundary conditions adopted in this study were

$$T = T_0 \text{ at } x = 0 \quad \text{(force boundary condition)} \tag{8a}$$

$$u = 0 \text{ at } x = L' \quad \text{(displacement boundary condition)} \tag{8b}$$

Use of a moving boundary condition in Eq. (8) and adoption of the constitutive relationships in Eqs. (1) and (2) lead to an explicit solution to the force equilibrium differential equation [Eq. (6)]. Specifically, the constants c_1 and c_2 in Eq. (7) result as follows:

$$c_1 = -\frac{T_0}{J_c} \tag{9a}$$

$$c_2 = \frac{T_0}{J_c}L' - \frac{\tau_y}{J_c}L'^2 \tag{9b}$$

Outcomes of the SGC Model

Substitution of the constants from Eq. (9) into Eq. (7) results in explicit solutions for u and du/dx:

$$\frac{du}{dx} = \frac{2\tau_y}{J_c}x - \frac{T_0}{J_c} \tag{10}$$

$$u = \frac{\tau_y}{J_c}x^2 - \frac{T_0}{J_c}x + \left(\frac{T_0}{J_c}L' - \frac{\tau_y}{J_c}L'^2\right) \tag{11}$$

Expressions for geosynthetic strain (ε) and unit tension (T) can also be obtained as follows:

$$\varepsilon = \frac{T_0}{J_c} - \frac{2\tau_y}{J_c}x \tag{12}$$

$$T = T_0 - 2\tau_y x \tag{13}$$

The interface shear stress, unit tension, relative displacement, and tensile strain predicted using the SGC model along the geosynthetic length are illustrated in Fig. 3. Specifically, Fig. 3(a) shows

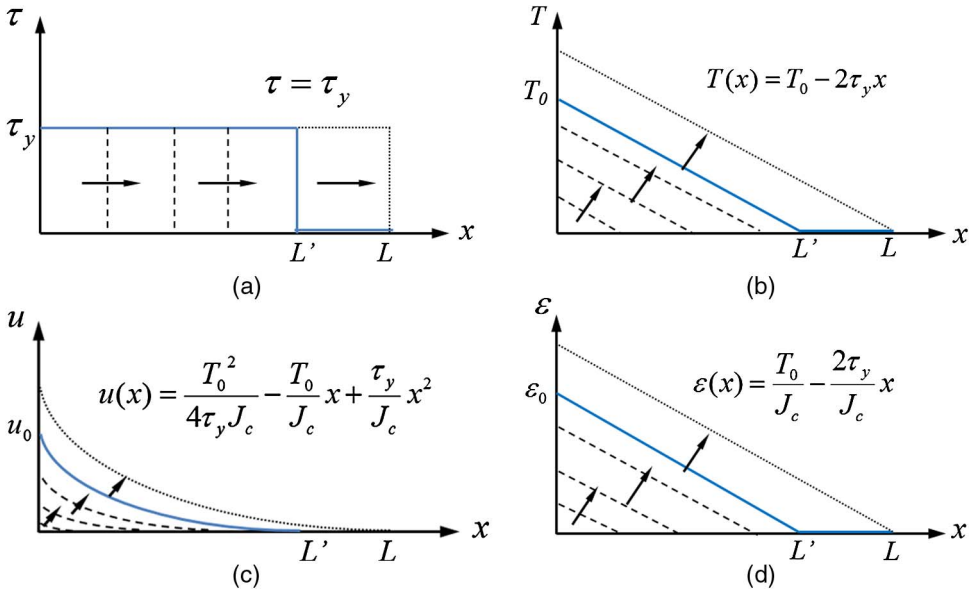

Fig. 3. Analytical predictions by the SGC model: (a) interface shear; (b) geosynthetic unit tension; (c) geosynthetic displacements; (d) geosynthetic strains

that the model predicts a uniform interface shear along the geosynthetic active length and zero shear beyond the active length. With increasing tension, the magnitude of the equivalent interface shear remains constant (and equal to τ_y), while the geosynthetic active length increases. The unit tension mobilized along the geosynthetic decreases linearly, from a maximum value T_0 at the frontal end to zero at the end of the active length [Fig. 3(b)]. The slope of this relationship equals $2\tau_y$. No tension is mobilized along the stationary portion of the geosynthetic. As inferred from Eq. (11), the displacements in a tensioned, extensible reinforcement follow a parabolic function, with the maximum value, u_0, at the loading front and zero at the end of the active length [Fig. 3(c)]. The coefficients of the parabola that represents the displacement function depend on the magnitude of the frontal unit tension, T_0, and the active length, L'. Finally, the tensile strains along the geosynthetic follow a linear relationship along the active length of the geosynthetic [Fig. 3(d)]. This relationship is proportional to the unit tension with a slope of $1/J_c$. The strain beyond the active length is zero.

Solving Eq. (13) at $x = L'$, and considering zero unit tension at the end of the active length (L'), results in

$$T_0 = 2\tau_y L' \tag{14}$$

Substituting this expression into Eqs. (11) and (13) yields Eqs. (15) and (16):

$$T_0 = 2\tau_y(L' - x) \tag{15a}$$

or

$$\frac{T}{2\tau_y} = (L' - x) \tag{15b}$$

$$u = \frac{\tau_y}{J_c}x^2 - \frac{2\tau_y L'}{J_c}x + \frac{\tau_y}{J_c}L'^2 \tag{16}$$

Eq. (16) can be rearranged as follows:

$$u = \frac{\tau_y}{J_c}(x^2 - 2L'x + L'^2) \tag{17a}$$

or

$$u\left(\frac{J_c}{\tau_y}\right) = (L' - x)^2 \tag{17b}$$

A comparison of Eqs. (15*b*) and (17*b*) results in

$$u\left(\frac{J_c}{\tau_y}\right) = \left(\frac{T}{2\tau_y}\right)^2 \tag{18}$$

Rearranging Eq. (18) results in a relevant expression that relates the unit tension at any location x (along the active length of the geosynthetic) to the corresponding displacement at that location, as follows:

$$T(x)^2 = (4J_c\tau_y) \cdot u(x) \tag{19}$$

Since the confined stiffness of the geosynthetic (J_c) and the yield shear stress (τ_y) are considered constants, the multiplier ($4\tau_y \cdot J_c$) is also constant. This constant represents a key parameter that may be particularly suitable to characterize of the soil–geosynthetic interaction under small displacements. This parameter is defined as the *stiffness of the soil–geosynthetic composite*, or K_{SGC}, as follows:

$$K_{SGC} = 4\tau_y J_c \tag{20}$$

That is

$$T(x)^2 = K_{SGC} \cdot u(x) \tag{21}$$

Eq. (21) indicates that a linear relationship can be defined between the geosynthetic displacement [$u(x)$] and the square of the unit tension [$T(x)^2$] at any location along the active length of the geosynthetic ($0 < x < L'$). The slope of this linear relationship is K_{SGC} [Fig. 4(a)]. Consequently, the SGC model results in a parabolic relationship between $T(x)$ and $u(x)$ under small displacements [Fig. 4(b)].

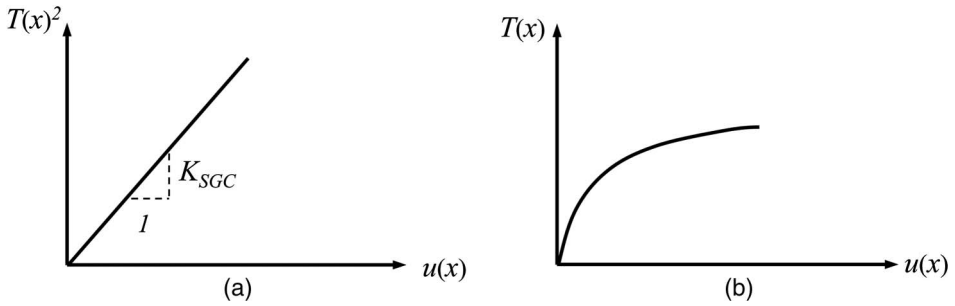

Fig. 4. Relationship between unit tension (T) and displacements (u) along active length of geosynthetic: (a) linear relationship between T^2 and u; (b) parabolic relationship between T and u

Experimental Evaluation of the Suitability of the SGC Model: Conceptual Approach

The interaction between soil and geosynthetics has typically been evaluated using interface direct shear as well as pullout tests, which mobilize the soil–geosynthetic interface in two fundamentally different modes (e.g., Abdi and Zandieh 2014; Sukmak et al. 2015; Weldu et al. 2016; Xiao et al. 2015). In the direct shear test, the soil placed in a half box is forced to slide, without mobilizing tension, over the geosynthetic specimen fixed to a block or to a second half box. In contrast, the geosynthetic specimen in a pullout test device is subjected to increasing tension and is pulled out of a soil mass that remains stationary under a constant confining pressure. The test continues until interface shear is mobilized along the entire embedded length of the geosynthetic (or until the geosynthetic breaks in tension if this condition occurs first). Unlike the direct shear test, where the geosynthetic is essentially fixed and does not elongate, the geosynthetic specimen in a pullout test is under tension and undergoes elongation while being pulled out of the soil. Accordingly, the relative displacements in a direct shear test result from imposing movement of the soil specimen over a stationary geosynthetic specimen, whereas the relative displacements in a pullout test result from imposing movement of the geosynthetic specimen while the soil remains stationary.

The soil–geosynthetic interaction device used in this study to characterize K_{SGC} allowed mobilization of shear along the soil–geosynthetic interface by mobilizing mechanisms similar to those developed in a conventional pullout test, although the focus was not on pullout resistance, but rather on measurements taken at the onset of geosynthetic mobilization. This experimental approach was adopted because it is representative of mechanisms relevant to practical applications involving geosynthetics, such as roadway base stabilization, that are governed by the initial stiffness of the soil-geosynthetic composite. The experimental procedures developed to evaluate the validity of the assumptions and outcomes of the SGC model are described conceptually in this section of the paper. The experimental results from a pilot test, as well as the values obtained for the key model parameters, are presented subsequently.

Experimental Setup for Soil–geosynthetic Interaction Testing

A series of soil–geosynthetic interaction tests were conducted in this study using equipment based on a pullout test device. Fig. 5 provides a schematic view of the test setup. Tests were conducted by embedding a geosynthetic specimen between two layers of soil, applying target normal pressure on top of the soil, and imposing a frontal displacement (or force) to the geosynthetic specimen. The corresponding frontal load was recorded at the front of the specimen, and the frontal load per unit width of the specimen corresponded to the frontal unit tension, T_0. Displacements in the geosynthetic specimen were also recorded at the loading front, u_0, as well as at several locations along the embedded length of the specimen (see displacements u_1 to u_5 in Fig. 5). Telltales were used along the embedded length of the geosynthetic to monitor the advancement of the mobilized length as the tests progressed.

Soil–geosynthetic interaction tests were terminated once one of the following termination criteria was satisfied: (1) the geosynthetic failed under tension, (2) a predetermined displacement was reached, or (3) an asymptote in the unit tension–displacement curve was reached, which was interpreted as corresponding to pullout failure. In addition, the frontal unit tension was recorded when

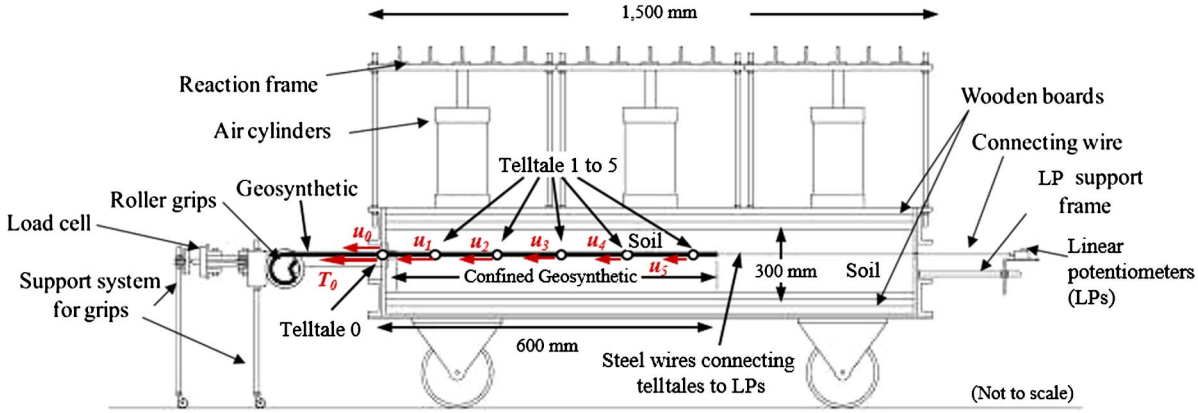

Fig. 5. Schematic view of equipment used for soil–geosynthetic interaction testing

the displacements at each telltale were first triggered. The onset of displacement, which was triggered at a different load level for each telltale, indicated the progressive mobilization of interface shear and resulted in increasing active length values. The first telltale was expected to be triggered by relatively small loads, while the rear telltales were triggered after increasingly larger load levels. The data recorded by telltales were utilized to define key parameters of the SGC model. These parameters included not only K_{SGC}, which was the main outcome of the test, but the two additional parameters that were used to define it as well, namely the yield interface shear stress (τ_y) and the confined geosynthetic stiffness (J_c) [Eq. (20)]. Experimental procedures were developed in this study to evaluate validity of the assumptions and outcomes of the SGC model and to determine the model parameters, as described in the next section of this paper. Additional details on these procedures are provided by Gupta (2009), Roodi (2016), and Zornberg et al. (2008).

Validation of the SGC Model: Linearity of the Relationship between Unit Tension Squared (T^2) and Displacements (u)

An important outcome of the analytical formulation developed in this study is the linearity of the relationship between the unit tension squared and the displacement at any point along the active length of the geosynthetic, as characterized by K_{SGC}. This section describes a procedure to experimentally evaluate the validity of this outcome by analyzing this relationship using the results of soil–geosynthetic interaction tests.

In the soil–geosynthetic interaction tests, the frontal unit tension (T_0) and displacements in the geosynthetic specimen at the location of the telltales are directly measured (Fig. 5). The unit tension in the geosynthetic at the location of each telltale can be estimated after considering the shear stress distribution assumed in the proposed model [Eq. (2)]. Since the interface shear is considered to develop progressively, the geosynthetic active length expands toward the free end of the geosynthetic. Considering a constant yield interface shear [Eq. (2)], the unit tension at a given point along the geosynthetic length could be estimated using the data measured from soil–geosynthetic interaction tests. Specifically, the unit tension T_i at the location of Telltale i can be obtained using measurements of the frontal unit tension collected when displacements at Telltale i are first triggered, $T_{0,i}$.

Considering force equilibrium from Eq. (13):

$$T_i = 0 \quad \text{if } T_0 < T_{0,i} \tag{22}$$

$$T_i = T_0 - T_{0,i} \quad \text{if } T_0 > T_{0,i} \tag{23}$$

Eq. (23) implies that after the active length reaches a given Point i, no additional shear stresses develop in the portion of the geosynthetic before that location (because the interface shear is assumed to be constant). Consequently, any additional tension results in the mobilization of shear beyond Point i.

In summary, the frontal unit tension that corresponds to the moment when displacements are first triggered in each telltale should be carefully recorded because this value is needed to define the unit tension at the location of each telltale. The frontal unit tension values are illustrated as a function of displacements in Fig. 6(a) for the case of Telltale i. The unit tension versus displacements at Location i [Fig. 6(b)] can be obtained by shifting the frontal unit tension versus displacement at that location by the amount of $T_{0,i}$. Consistent with the model proposed in this study, this curve should define a parabola under small displacements. The unit tension–displacement data can be converted into the T^2 versus u space by squaring the unit tension values [Fig. 6(c)]. According to the model, the experimental data in the T^2 versus u space should define a straight line with slope K_{SGC}.

Validation of the SGC Model: Uniqueness of K_{SGC}

The analytical model predicts that the linear relationship between the geosynthetic unit tension and the displacement is unique and independent of location within the geosynthetic. Specifically, the value estimated for K_{SGC} should be the same at any point along the active length of the geosynthetic. Displacement measurements at various points along the geosynthetic should then produce data that can be used to experimentally validate this outcome of the model.

A total of five telltales were installed along the embedded specimen with the first (Telltale 1) situated close to the loading front and the last (Telltale 5) situated close to the free end. The displacement data recorded by each telltale can be used according to the procedure described in the previous section to obtain the relationship between the unit tension squared and displacement at the location of that telltale. As illustrated in Fig. 7, the uniqueness of K_{SGC} can be explored by comparing the lines defined using data from the various telltales. The analytical model predicts that the slopes of the lines should be the same.

Validation of the SGC Model: Suitability of Constitutive Relationships

The results from the soil–geosynthetic interaction tests can also be used to define the yield shear stress (τ_y) and the confined stiffness of the geosynthetic (J_c). As illustrated in Fig. 8, because displacements in the geosynthetic are measured at the locations of the telltales, the average strain between these locations can be calculated at any given time, as follows:

$$\varepsilon_{\text{avg}\,ij} = \frac{u_i - u_j}{L_{ij}} \tag{24}$$

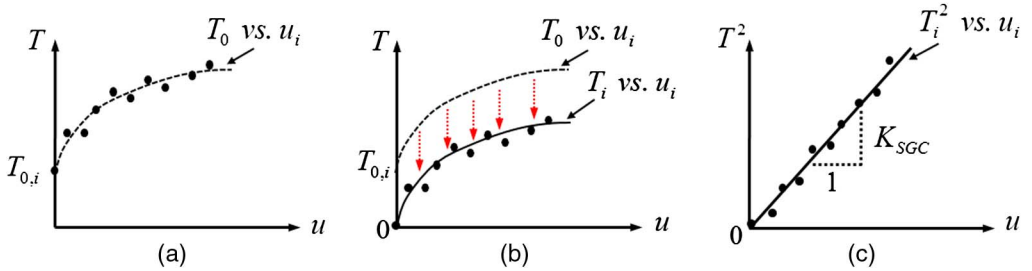

Fig. 6. Schematic view of steps in the procedure developed to estimate K_{SGC}: (a) frontal unit tension versus Telltale i displacement; (b) unit tension at Point i versus Telltale i displacement; (c) unit tension squared at Point i versus Telltale i displacement

J. Geotech. Geoenviron. Eng., 2017, 143(10): 04017075

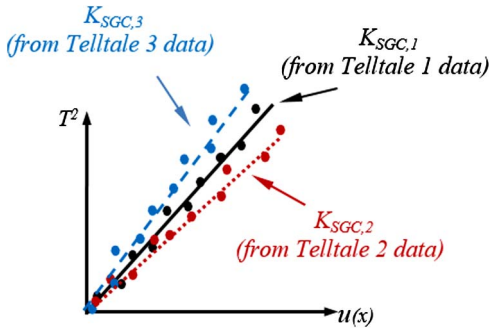

Fig. 7. Experimental evaluation of uniqueness of K_{SGC}

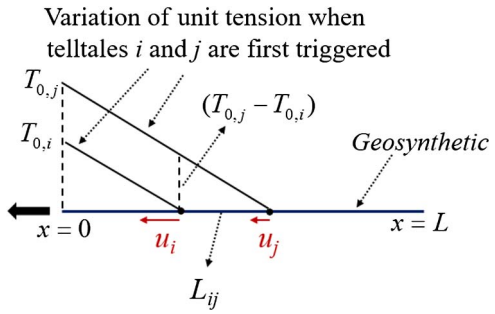

Fig. 8. Estimation of $\varepsilon_{avg\,ij}$ and $T_{avg\,ij}$ from soil–geosynthetic test results

where u_i = displacement at Telltale i at a given time; u_j = displacement at Telltale j at the same time; and L_{ij} = distance between locations of Telltales i and j. The average unit tension in the portion of the geosynthetic between Points i and j can also be determined. Specifically, this tension can be defined at the time when each telltale is first triggered, which is when the displacement beyond each of the telltales is zero. In this case, the average unit tension in the segment, $T_{avg\,ij}$, can be calculated as follows:

$$T_{avg\ ij} = \frac{T_{0,j} - T_{0,i}}{2} \tag{25}$$

As illustrated in Fig. 9, estimation of $\varepsilon_{avg\,ij}$ and $T_{avg\,ij}$ between multiple telltale locations allows determination of the geosynthetic unit tension versus strain relationship, the slope of which represents the confined stiffness of the geosynthetic.

Determination of τ_y can also be achieved following the illustration in Fig. 10. Since a uniform distribution is assumed for the equivalent interface shear (τ_y), the equilibrium of forces along

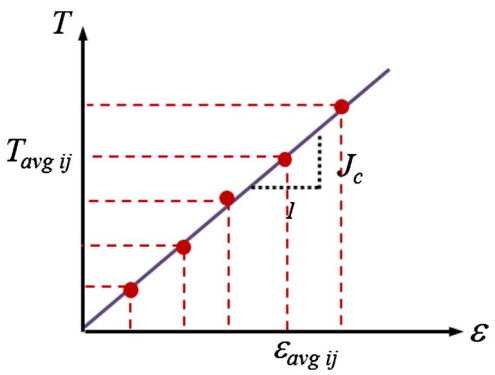

Fig. 9. Estimation of J_c using soil–geosynthetic interaction test results

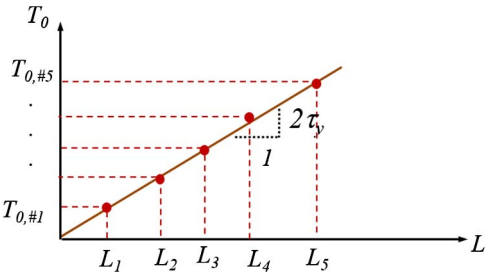

Fig. 10. Estimation of τ_y from soil–geosynthetic test results

the active length (L_i') can be described by Eq. (14). Therefore, τ_y is obtained as

$$\tau_y = \frac{T_{0,i}}{2L'_i} \tag{26}$$

When Telltale i is first triggered, the recorded frontal unit tension corresponds to $T_{0,i}$ and the location of the telltale corresponds to the active length (L_i'). Therefore, multiple realizations of $T_{0,i}$ and L_i' can be obtained for multiple telltales. According to the SGC model, the relationships between $T_{0,i}$ and L_i' should result in a straight line with the slope $2\tau_y$, as illustrated in Fig. 10.

Representation of Displacements along Embedment Length

An alternative procedure to determine the parameters of the proposed model involves direct use of geosynthetic displacements along the active length. As previously described, the SGC model predicts a family of parabolic functions for the displacements along the active length of the geosynthetic. As illustrated in Fig. 3, for a given frontal unit tension, displacements are represented by a parabolic function that depends solely on τ_y and J_c. Therefore, a polynomial regression can be used to estimate the equation coefficients. In this regression, the values of τ_y and J_c can be optimized to define the best fit to the experimental data (Fig. 11). The best fit is identified using the least-squares approach, which involves minimizing the sum of the squares of the errors between the experimental data and predictions. Specifically, the values of τ_y and J_c that minimize the error for the family of parabolic curves can be defined.

For any given value of T_0 (including the values of $T_{0,i}$) the sum of the squares of the errors, S_i, is expressed as follows:

$$S_i = \sum_{j=1}^{n} r_{ji}^2 \tag{27}$$

$$r_{ji} = u_{ji,e} - u_{ji,p} \tag{28}$$

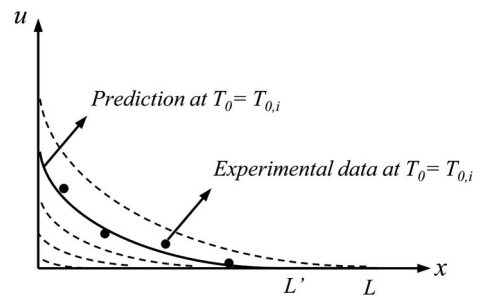

Fig. 11. Estimation of τ_y and J_c from parabolic regression of telltale displacements

where n = number of telltales; r_{ji} = residual between predicted and measured displacements; $u_{ji,e}$ = experimental value for displacement recorded at Telltale j when the frontal unit tension is $T_{0,i}$; and $u_{ji,p}$ = predicted value for displacement at Telltale j when the frontal unit tension is $T_{0,i}$. The total sum of the squares of the errors, S, results from integrating S_i over the range of $T_{0,i}$ values that resulted in the displacements used to estimate K_{SGC}.

It should be noted that the various procedures described herein are expected to result in the same model parameters. However, discrepancies can be expected due to assumptions in the theory and scatters in the experimental measurements. As described in the next section, comparison between the parameters obtained using the various procedures allowed evaluation of the suitability of the model and provided insight into the variability of the various parameters.

Experimental Evaluation of the Suitability of the SGC Model: Pilot Test Results

The results of a pilot large-scale soil–geosynthetic interaction test are presented herein to evaluate the suitability of the constitutive relationships and outcomes of the proposed SGC model. The approaches conceptually detailed in the previous section were used to interpret the experimental data obtained in this pilot test in order to assess the consistency of the data trends with model predictions as well as to estimate K_{SGC}, τ_y, and J_c. The pilot test was conducted using the large-scale soil–geosynthetic interaction device illustrated in Fig. 5. The characteristics of this device are provided in the companion paper.

Pilot Test Characteristics

The backfill material used in the pilot test consisted of a clean poorly graded sand, known as Monterey No. 30 sand (Zornberg et al. 1998b). This backfill material was used because of the relatively small variation in its characteristics that has made it a standard soil in previous studies. The sand has a uniform soil particle size distribution, with particle sizes smaller than 0.762 mm, and is composed of medium to fine and subangular to subrounded particles. The mean particle size (D_{50}), coefficient of uniformity (C_u), and coefficient of curvature (C_c) were determined to be 0.44 mm, 1.6, and 1.0, respectively. Monterey No. 30 sand is classified as poorly graded sand, according to the Unified Soil Classification System (USCS) [ASTM D2487 (ASTM 2011)], and as Group A-1-b, according to the AASHTO classification system [AASHTO M145 (AASHTO 2012); ASTM D3282 (ASTM 2015)]. The sand was placed with a moisture content of 1.5–2% and compacted in four lifts of 75 mm to reach a total thickness of 280 mm (after compaction) and a dry unit weight of 14.94 kN/m^3 after compaction.

Testing was conducted using a normal pressure of 21 kPa. Biaxial geogrids have often been used in roadway systems, which require deformability or serviceability criteria in their design. Accordingly, a commercially available biaxial geogrid was used as the geosynthetic inclusion. The aperture dimensions of the geogrid were 25 and 33 mm, while its minimum rib thickness was 0.76 mm in both directions. The aperture stability of the geogrid was 0.32 m-N/ deg, and the aspect ratio of the geogrid ribs was 0.23 in both directions. The confined portion of the specimen, tested in the cross-machine direction, was 320 mm wide and 1,020 mm long (embedded length). The unconfined tensile modulus of the geogrid, reported at 2 and 5% strain, was 330 and 268 kN/m, respectively, in the cross-machine direction and 205 and 170 kN/m, respectively, in the machine direction.

As schematically illustrated in Fig. 12, five telltales were attached to five geogrid junctions along its embedded portion at distances of 60, 180, 300, 410, and 850 mm from the loading front. The telltales consisted of cobalt-based alloy wires, 0.41 mm in diameter. The wires were tied at specific geogrid junctions, tightened by crimping their ends inside aluminum ferrules, and inserted into high-strength plastic tubes to minimize direct contact with the surrounding soil (Roodi 2016). The telltales were connected to five linear potentiometers (LPs) installed in the back of the box. An additional telltale was attached to one of the first junctions in the unconfined portion of the geogrid (Telltale 0 in Fig. 12) to measure frontal displacements.

Fig. 13 shows the measured frontal load and frontal displacements, as well as the telltale displacements along the confined length. Progressive development of interface shear is clearly observed in the data presented in this figure. LP 1, connected to the telltale closest to the pulling front, was triggered at a relatively low frontal unit tension. The subsequent LPs were triggered in the order of their location within the geosynthetic specimen. That is, as the frontal unit tension increased, LPs 2, 3, and 4 were successively triggered. The test was terminated once the geosynthetic specimen was observed to break under tension outside of the confined area. Breakage occurred before displacements were recorded by LP 5, which indicates that the active length of the geosynthetic did not reach the location of Telltale 5. Therefore, the end portion of the geosynthetic had indeed remained stationary.

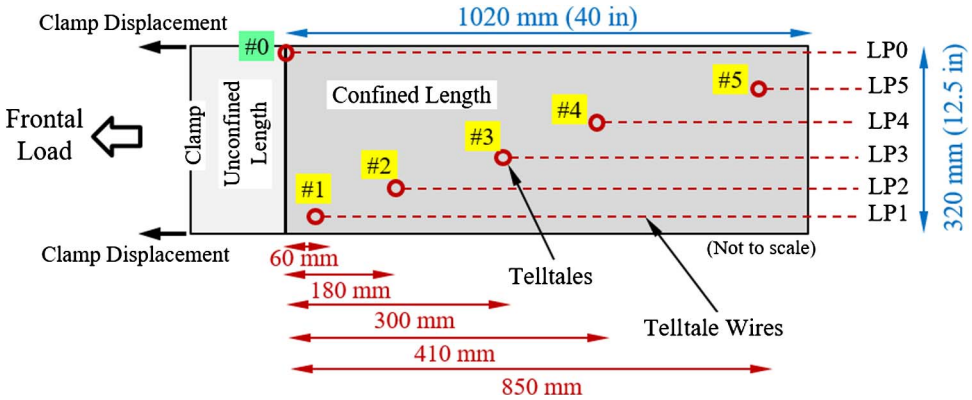

Fig. 12. Schematic view of geosynthetic specimen and telltale setup

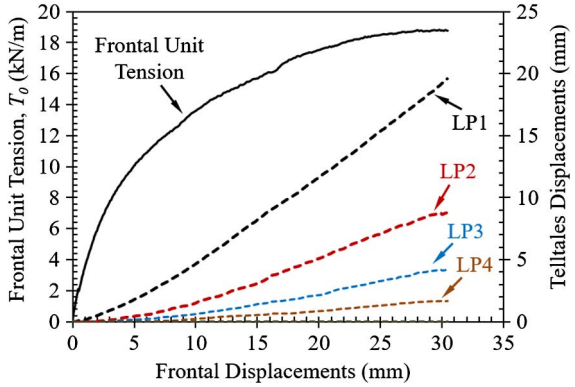

Fig. 13. Results of the pilot large-scale soil–geosynthetic interaction test: frontal load and telltale displacements versus frontal displacement

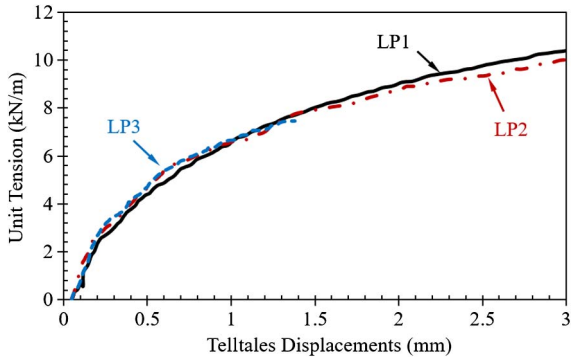

Fig. 14. Representation of unit tension (T) versus displacements (u) data for telltales

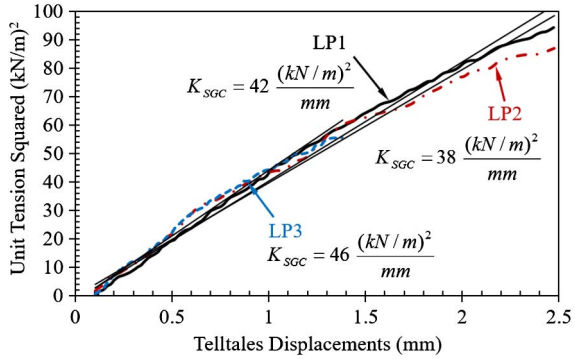

Fig. 15. Evaluation of the linearity and uniqueness of unit tension squared (T^2) versus displacement (u) data

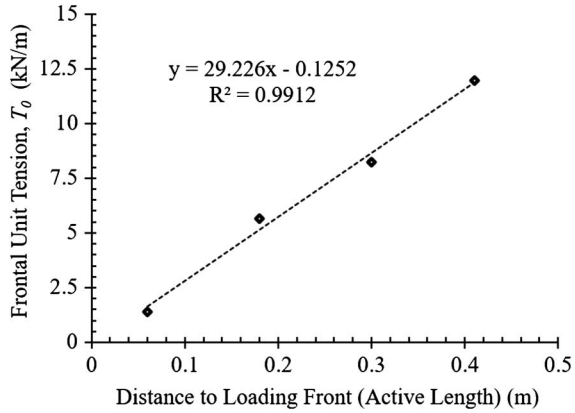

Fig. 16. Experimental evaluation of the validity of the constitutive model adopted for soil–geosynthetic interface shear

Evaluation of the Linearity and Uniqueness of Unit Tension Squared (T^2) versus Displacement (u) Data

The unit tension versus displacement data for the three frontal telltales (i.e., Telltales 1, 2, and 3) is presented in Fig. 14. As described in the previous section, these data were obtained after plotting and shifting the frontal unit tension versus telltale displacement data presented in Fig. 13. Consistent with the predictions of the analytical model, which assumed constant values for yield interface shear and confined geosynthetic stiffness, the shape of T versus u data was found to be essentially the same for the different points along the active length of the geosynthetic. Specifically, the three unit tension (T) versus displacement (u) curves in Fig. 14 were essentially situated on top of each other and define a parabola for the range of displacements evaluated in this study. The experimental data presented in Fig. 14 verify the uniqueness of the unit tension versus displacement relationship, as predicted by the SGC model.

The unit tension squared (T^2) versus displacement (u) data was then obtained (Fig. 15). Consistent with the predictions of the SGC model, the experimental data presented in Fig. 15 confirm the linear relationship between the unit tension squared (T^2) and telltale displacements (u) for all three telltales. Furthermore, the lines defined by the data obtained from the three telltales exhibited reasonably similar slopes, which further underscored the uniqueness of the linear relationship between the unit tension squared (T^2) and displacements (u) throughout the active length of the specimen.

The stiffness of the soil–geosynthetic composite (K_{SGC}) was estimated as the slope of the T^2 versus u data. As illustrated in Fig. 15, the K_{SGC} value estimated by the data obtained from the three telltales ranged from 38 to 46 $(kN/m)^2/mm$. It should be noted that the unit tensions calculated in Fig. 15 were used only to evaluate the linearity and uniqueness of the T^2 versus u relationship. However, as presented next, validation of other aspects of the model relies on measurement of the frontal unit tension at the time when each telltale is first triggered.

Evaluation of the Constitutive Relationships Adopted for the SGC Model

The experimental data obtained in the pilot test was also used to evaluate the suitability of the constitutive relationships assumed in the SGC model. Fig. 16 shows the frontal unit tension when displacements at Telltales 1–4 were first triggered versus the locations of the telltales within the active geosynthetic length. The linearity of the correlation observed in this figure provides additional evidence of the suitability of the constitutive model assumed for soil–geosynthetic interface shear, at least for comparatively small displacements. Accordingly, the yield interface shear corresponds to half of the slope of this linear relationship ($\tau_y = 29.2/2 = 14.6$ kN/m^2).

The suitability of the constitutive relationship adopted for the geosynthetic [Eq. (1)] was also assessed. As previously described, the average geosynthetic strain and unit tension were estimated at the times when displacements at telltales were first triggered. This information allowed evaluation of the confined stiffness of the geosynthetic specimen. Since the confined data points were calculated for comparatively small displacements, the predicted strain values remained below 1%. As shown in Fig. 17, the confined data shows a linear trend between geosynthetic unit tension and strain,

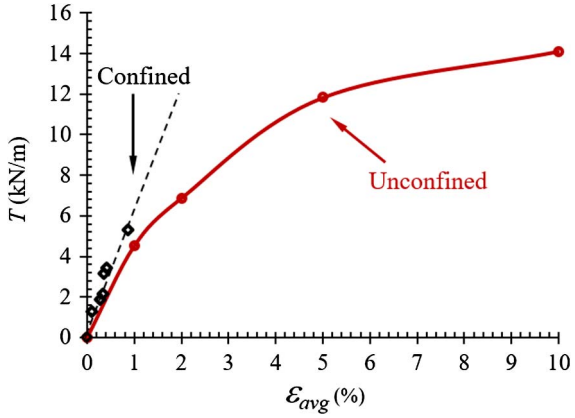

Fig. 17. Experimental evaluation of the validity of the constitutive model adopted for geosynthetic material

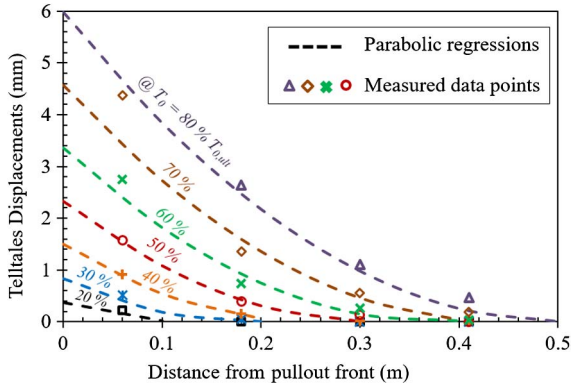

Fig. 18. Parabolic representation of displacement data from telltales

confirming the suitability of the constitutive model adopted in the SGC model for geosynthetic materials. Conventional wide-width tensile tests were also conducted on the geosynthetic to evaluate its stiffness under unconfined conditions. Comparison of the tension data for confined and unconfined conditions is provided in Fig. 17. The initial slope of the unit tension versus strain data obtained from unconfined tests showed reasonably good agreement with the slope of the data from confined conditions. Specifically, the slope in the confined conditions characterized the confined geosynthetic stiffness as $J_c = 660$ kN/m.

As previously discussed, the constitutive parameters of the SGC model, τ_y and J_c, can also be estimated from a parabolic regression of telltale displacement data. Fig. 18 presents the family of parabolas obtained by fitting the experimental data recorded in the pilot soil–geosynthetic interaction test. Since the model was developed considering small displacements, only displacements below 2.5 mm were used in the regression analysis. Displacements that were recorded when the frontal load exceeded 80% of the ultimate frontal load were also not considered. The regression analysis resulted in a yield shear stress (τ_y) of 14.9 kN/m^2, a confined geosynthetic stiffness (J_c) of 630 kN/m, and a sum of the squared residuals (S) of 6.9 mm^2. Very good consistency can be observed between the τ_y and J_c values obtained from the parabolic regression and those previously obtained using separate procedures. This provides additional evidence of the suitability of the constitutive relationships adopted in the SGC model.

The regression results can also be used in Eq. (20) to estimate the stiffness of the soil-geosynthetic composite as $K_{SGC} = 4\tau_y \cdot J_c = 38(\text{kN/m})^2/\text{mm}$. This value is well within the range of the values obtained directly from defining the slope of the T^2 versus u data.

Summary and Conclusions

A new model, referred to as the soil-geosynthetic composite (SGC) model, was proposed to evaluate the interaction between soil and geosynthetics under small displacements. Although previously developed models have often focused on characterizing the resistance of soil–geosynthetic systems, the proposed model emphasizes characterization of the stiffness of these systems. Such characterization is relevant to projects such as the base stabilization of roadways, where design is based on deformability criteria. A relevant feature of the new model is that it defines the stiffness of soil-geosynthetic composite using a single parameter, which makes it particularly suitable for practical applications (e.g., for specification or for mechanistic-empirical formulations). The model was derived considering a force equilibrium differential equation by adopting a moving domain for the boundary conditions and by assuming two constitutive relationships: (1) a linear relationship between the unit tension and tensile strain in the geosynthetic, characterized by J_c, the confined geosynthetic stiffness; and (2) a rigid–perfectly plastic relationship between the interface shear and geosynthetic displacements, characterized by the yield interface shear stress, τ_y. Specific experimental procedures were developed to determine model parameters using soil–geosynthetic interaction tests. Although the soil–geosynthetic interaction equipment used in this study was based on a large-scale pullout device, emphasis was placed on the interpretation of the displacement data along the active length of the geosynthetic. The results from a pilot test were used to assess the suitability of the constitutive relationships and outcomes of the SGC model. The main findings that result from the analytical and experimental evaluations conducted in this study are summarized as follows:

- A closed-form analytical solution could be obtained for the soil–geosynthetic force equilibrium differential equation. This required use of a linear constitutive relationship for the confined geosynthetic, a rigid–perfectly plastic relationship for the interface shear, and a specific moving boundary condition.
- The closed-form solution of the SGC model is characterized by a single parameter, the stiffness of the soil-geosynthetic composite (K_{SGC}). The K_{SGC} value is representative of a given soil-geosynthetic composite system, under a certain confining pressure, because it captures both the tensile characteristics of the confined geosynthetic and the shear behavior of the soil–geosynthetic interface.
- Experimental testing procedures could be defined to unambiguously obtain the K_{SGC} parameter. They require determination of the frontal unit tension, internal displacements, and the frontal unit tension when the displacements are first mobilized within an embedded geosynthetic.
- The K_{SGC} parameter is defined as the slope of the line between the unit tension squared (T^2) and displacements (u) along the embedded length of the geosynthetic. The linearity of the relationship between the unit tension squared (T^2) and displacements (u) was experimentally validated using the results from a pilot soil–geosynthetic interaction test. The pilot test presented in this paper was conducted using large-scale soil–geosynthetic interaction equipment to test a biaxial geogrid in the cross-machine direction.
- The uniqueness of the K_{SGC} parameter was experimentally validated. Specifically, the same K_{SGC} was obtained, independent of the location within the embedded geosynthetic, where the

experimental data (displacements from telltales) was collected as the test progressed.
- Evaluation of the experimental results from the pilot test also confirmed the suitability of the constitutive relationships adopted in this study to characterize the geosynthetic and the soil–geosynthetic interface shear under small displacements.

Overall, the availability of a single parameter, K_{SGC}, to characterize the initial stiffness of a soil-geosynthetic composite may be particularly relevant for practical applications, such as the base stabilization of roadways. A companion paper evaluates the suitability of the constitutive assumptions and outcomes of the model for a range of variables that may affect the predictions of the SGC model (Roodi and Zornberg 2017).

Acknowledgments

The authors are grateful for the financial support received from the Texas Department of Transportation.

Notation

The following symbols are used in this paper:

c_1 = constant of integration;
c_2 = constant of integration;
E = elastic modulus;
J_c = confined geosynthetic stiffness;
K_{SGC} = stiffness of soil–geosynthetic composite;
L = embedment length of geosynthetic;
L' = active length of geosynthetic;
L_{ij} = distance between locations of Telltales i and j;
r_{ji} = residual between predicted and measured displacements;
S = total sum of squares of error;
S_i = sum of squares of error;
T = unit tension;
T_0 = frontal unit tension;
$T_{0,i}$ = frontal unit tension at the time displacements at Telltale i are first triggered;
$T_{\text{avg}\,ij}$ = average unit tension in geosynthetic between locations of Telltales i and j;
T_i = unit tension at location of Telltale i;
t = thickness;
u = displacement;
u_0 = frontal displacement;
u_i = displacement at location of Telltale i;
$u_{ji,e}$ = experimental value for displacement recorded at Telltale j when $T_0 = T_{0,i}$;
$u_{ji,p}$ = predicted value for displacement recorded at Telltale j when $T_0 = T_{0,i}$;
x = distance from loading front;
ε = tensile strain;
ε_0 = frontal tensile strain;
$\varepsilon_{\text{avg}\,ij}$ = average tensile strain between locations of Telltales i and j;
τ = interface shear stress; and
τ_y = yield interface shear stress.

References

AASHTO. (2012). "Standard specification for classification of soils and soil-aggregate mixtures for highway construction purposes." *AASHTO M145-91(12)*, Washington, DC.

Abdesssemed, M., Kenai, S., and Bali, A. (2015). "Experimental and numerical analysis of the behavior of an airport pavement reinforced by geogrids." *Constr. Build. Mater.*, 94(Sep), 547–554.

Abdi, M. R., and Zandieh, A. R. (2014). "Experimental and numerical analysis of large scale pull out tests conducted on clays reinforced with geogrids encapsulated with coarse material." *Geotext. Geomembr.*, 42(5), 494–504.

Allen, T. M., Christopher, B. R., and Holtz, R. D. (1992). "Performance of a 12.6 m high geotextile wall in Seattle, Washington." *Proc., Int. Symp. on Geosynthetic-Reinforced Soil Retaining Walls*, J. T. H. Wu, ed., A.A. Balkema, Rotterdam, Netherlands, 81–100.

Alobaidi, I. M., Hoare, D. J., and Ghataora, G. S. (1997). "Load transfer mechanism in pull-out tests." *Geosynth. Int.*, 4(5), 509–521.

Al-Qadi, I. L., Dessouky, S. H., Kwon, J., and Tutumluer, E. (2008). "Geogrid in flexible pavements: Validated mechanism." *Transp. Res. Rec.*, 2045, 102–109.

Archer, S., and Wayne, M. H. (2012). "Relevancy of material properties in predicting the performance of geogrid-stabilized roadway." *Proc., Geo-Congress 2012: State of the Art and Practice in Geotechnical Engineering*, ASCE, Reston, VA, 1320–1329.

ASTM. (2011). "Standard practice for classification of soils for engineering purposes (unified soil classification system)." *ASTM D2487-11*, West Conshohocken, PA.

ASTM. (2015). "Standard practice for classification of soils and soil-aggregate mixtures for highway construction purposes." *ASTM D3282-15*, West Conshohocken, PA.

Bergado, D. T., and Chai, J. C. (1994). "Pullout force-displacement relationship of extensible grid reinforcements." *Geotext. Geomembr.*, 13(5), 295–316.

Biabani, M. M., and Indraratna, B. (2015). "An evaluation of the interface behaviour of rail subballast stabilised with geogrids and geomembranes." *Geotext. Geomembr.*, 43(3), 240–249.

Chen, Q., and Abu-Farsakh, M. (2012). "Structural contribution of geogrid reinforcement in pavement." *Proc., Geo-Congress 2012: State of the Art and Practice in Geotechnical Engineering*, ASCE, Reston, VA, 1468–1475.

Christopher, B. R., Cuelho, E. V., and Perkins, S. W. (2008). "Development of geogrid junction strength requirement for reinforced roadway base design." *Proc., GeoAmericas 2008*, Industrial Fabrics Association International, St. Paul, MN, 1003–1012.

Christopher, B. R., Holtz, R. D., and Bell, W. D. (1986). "New tests for determining the in-soil stress-strain properties of geotextiles." *Proc., 3rd Int. Conf. on Geotextiles*, International Society of Soil Mechanics and Foundation Engineering, U.K., 683–686.

Cuelho, E. V., and Perkins, S. W. (2009). "Field investigation of geosynthetics used for subgrade stabilization." *Rep. FHWA/MT-09-0003/8193*, Montana DOT, MT.

El-Fermaoui, A., and Nowatzki, E. (1982). "Effect of confining pressure on performance of geotextiles in soils." *Proc., 2nd Int. Conf. on Geotextiles*, Industrial Fabrics Association International, St. Paul, MN, 799–804.

Giroud, J. P., and Han, J. (2004a). "Design method for geogrid-reinforced unpaved roads. I: Theoretical development." *J. Geotech. Geoenviron. Eng.*, 10.1061/(ASCE)1090-0241(2004)130:8(775), 776–786.

Giroud, J. P., and Han, J. (2004b). "Design method for geogrid-reinforced unpaved roads. II: Calibration and verification." *J. Geotech. Geoenviron. Eng.*, 10.1061/(ASCE)1090-0241(2004)130:8(787), 787–797.

Gu, M., Zhao, M., Zhang, L., and Han, J. (2016). "Effects of geogrid encasement on lateral and vertical deformations of stone columns in model tests." *Geosynth. Int.*, 23(2), 100–112.

Gupta, R. (2009). "A study of geosynthetic-reinforced flexible pavement system." Ph.D. dissertation, Univ. of Texas, Austin, TX.

Gurung, N., and Iwao, Y. (1999). "Comparative model study of geosynthetic pull-out response." *Geosynth. Int.*, 6(1), 53–68.

Han, J., and Thakur, J. K. (2015). "Sustainable roadway construction using recycled aggregates with geosynthetics." *Sustainable Cities Soc.*, 14(Feb), 342–350.

Hanumasagar, S. S., Roodi, G. H., Zornberg, J. G., and Grubb, D. G. (2014). "Pullout characterization of geogrids embedded in dredged material and steel slag fines (DM-SSF) blends." *Proc., 10th Int. Conf.*

on Geosynthetics, 10ICG 2014, International Geosynthetics Society, Jupiter, FL.
Jewell, R. A. (1996). *Soil reinforcement with geotextiles*, Thomas Telford, London.
Jewell, R. A., Milligan, G. W. E., Sarsby, R. W., and Dubois, D. (1984). "Interaction between soil and geogrids." *Proc., Symp. on Polymer Grid Reinforcement in Civil Engineering*, Science and Engineering Research Council and Netlon Limited, Thomas Telford, London, 18–30.
Juran, I., and Chen, C. L. (1988). "Soil-geotextile pull-out interaction properties: Testing and interpretation." *Transp. Res. Rec.*, 1188, 37–47.
Kokkalis, A., and Papacharisis, N. (1989). "A simple laboratory method to estimate the in-soil behavior of geotextiles." *Geotext. Geomembr.*, 8(2), 147–157.
Leshchinsky, D., and Field, D. A. (1987). "In-soil load elongation tensile strength and interface friction of nonwoven geotextiles." *Proc., Geosynthetics '87*, Vol. 1, Industrial Fabrics Association International, St. Paul, MN, 238–249.
Matsui, T., San, K. C., Nabeshima, Y., and Amin, U. N. (1996). "Bearing mechanism of steel reinforcement in pull-out test." *Proc., Int. Symp. on Earth Reinforcement*, Balkema, Fukuoka, Japan.
McGown, A., Andrawes, K. Z., and Kabir, M. H. (1982). "Load-extension testing of geotextiles confined in soil." *Proc., 2nd Int. Conf. on Geotextiles*, Industrial Fabrics Association International, St. Paul, MN, 793–798.
Mendes, M. J. A., Palmeira, E. M., and Matheus, E. (2007). "Some factors affecting the in-soil load-strain behaviour of virgin and damaged nonwoven geotextiles." *Geosynth. Int.*, 14(1), 39–50.
Palmeira, E. M. (2009). "Soil-geosynthetic interaction: Modelling and analysis." *Geotext. Geomembr.*, 27(5), 368–390.
Palmeira, E. M., and Milligan, G. W. E. (1989). "Scale and other factors affecting the results of pull-out tests of grid buried in sand." *Geotechnique*, 39(3), 511–524.
Palmeira, E. M., Tupa, N., and Gomes, R. C. (1996). "In-soil tensile behaviour of geotextiles confined by fine soils." *Proc., Int. Symp. on Earth Reinforcement, IS Kyushu-96*, A.A. Balkema, Rotterdam, Netherlands, 129–132.
Pando, M. A., Swan, R. H., Park, Y., and Sheridan, S. (2014). "Experimental study of bottom coal ash-geogrid interaction." *Proc., Geo-Congress 2014: Geo-Characterization and Modeling for Sustainability*, ASCE, Reston, VA, 316–325.
Perkins, S. W., et al. (2004). "Development of design methods for geosynthetic reinforced flexile pavements." *Final Rep. FHWA-DTFH61-01-X-00068*, U.S. DOT, Federal Highway Administration, Washington, DC.
Perkins, S. W., and Cuelho, E. V. (1999). "Soil-geosynthetic interface strength and stiffness relationships from pullout tests." *Geosynth. Int.*, 6(5), 321–346.
Peterson, L. M., and Anderson, L. R. (1980). "Pullout resistance of welded wire mats embedded in soil." *Rep. to Hilfiker Co.*, Civil Environment Engineering Dept., Utah State Univ., Logan, UT.
Roodi, G. H. (2016). "Analytical, experimental, and field evaluations of soil-geosynthetic interaction under small displacements." Ph.D. dissertation, Univ. of Texas, Austin, TX.
Roodi, G. H., and Zornberg, J. G. (2012). "Effect of geosynthetic reinforcements on mitigation of environmentally induced cracks in pavements." *Proc., EuroGeo5: 5th European Geosynthetics Conf.*, R. B. Servicios Editoriales, Spain, 611–616.
Roodi, G. H., and Zornberg, J. G. (2017). "Stiffness of soil-geosynthetic composite under small displacements. II: Experimental evaluation." *J. Geotech. Geoenviron. Eng.*, 10.1061/(ASCE)GT.1943-5606.0001769, 04017076.
Schlosser, F., and Long, N. T. (1973). "Recent results in French research on reinforced soil." *J. Constr. Eng.*, 100(3), 223–237.
Sieira, A. C. C. F., Gerscovich, D. M. S., and Sayao, A. S. F. J. (2009). "Displacement and load transfer mechanisms of geogrids under pullout condition." *Geotext. Geomembr.*, 27(4), 241–253.
Siel, B. D., Tzong, W. H., and Chou, N. N. S. (1987). "In-soil stress-strain behavior of geotextile." *Proc., Geosynthetics '87*, Industrial Fabrics Association International, St. Paul, MN, 260–265.
Sobhi, S., and Wu, J. T. H. (1996). "Interface pullout formula for extensible sheet reinforcement." *Geosynth. Int.*, 3(5), 565–582.
Sukmak, K., Sukmak, P., Horpibulsuk, S., Han, J., Shen, S., and Arulrajah, A. (2015). "Effect of fine content on the pullout resistance mechanism of bearing reinforcement embedded in cohesive–frictional soils." *Geotext. Geomembr.*, 43(2), 107–117.
Swan, R. H., and Yuan, Z. (2013a). "Tensile behavior of triaxial geogrid: Application of the theoretical method." *Proc., Geosynthetics 2013*, Industrial Fabrics Association International, St. Paul, MN, 424–433.
Swan, R. H., and Yuan, Z. (2013b). "Tensile behavior of triaxial geogrid: Development of a theoretical method." *Proc., Geosynthetics 2013*, Industrial Fabrics Association International, St. Paul, MN, 434–443.
Terzaghi, K. (1943). *Theoretical soil mechanics*, Wiley, New York.
Vesic, A. S. (1963). "Bearing capacity of deep foundations in sand." *Highway Res. Rec.*, 39, 112–153.
Weerasekara, L., and Wijewickreme, D. (2010). "An analytical method to predict the pullout response of geotextiles." *Geosynth. Int.*, 17(4), 193–206.
Weldu, M. T., Han, J., Rahmaninezhad, S. M., Parsons, R. L., Kakrasul, J. I., and Jiang, Y. (2016). "Effect of aggregate uniformity on pullout resistance of steel strip reinforcement." *Transp. Res. Rec.*, 2579, 1–7.
Wilson-Fahmy, R. F., and Koerner, R. M. (1993). "Finite element modeling of soil-geogrid interaction with application to the behavior of geogrids in a pullout loading condition." *Geotext. Geomembr.*, 12(5), 479–501.
Wu, J. T. H. (1991). "Measuring inherent load-extension properties of geotextiles for design of reinforced structures." *Geotech. Test. J.*, 14(2), 157–165.
Xiao, M., Ledezma, M., and Hartman, C. (2015). "Shear resistance of tire-derived aggregate using large-scale direct shear tests." *J. Mater. Civil Eng.*, 10.1061/(ASCE)MT.1943-5533.0001007, 04014110.
Yang, Z. Z. (1972). "Strength and deformation characteristics of reinforced sand." Ph.D. dissertation, Univ. of California, Los Angeles.
Yuan, Z. (2011). "Pullout response of geosynthetic in soil-theoretical analysis." *Proc., Geo-Frontiers 2011: Advances in Geotechnical Engineering*, ASCE, Reston, VA, 4388–4397.
Zornberg, J. G., et al. (2008). "Validating mechanisms in geosynthetic reinforced pavements." *Rep. FHWA/TX-08/0-4829-1*, Texas DOT, Austin, TX.
Zornberg, J. G., and Arriaga, F. (2003). "Strain distribution within geosynthetic-reinforced slopes." *J. Geotech. Geoenviron. Eng.*, 10.1061/(ASCE)1090-0241(2003)129:1(32), 32–45.
Zornberg, J. G., Ferreira, J. A. Z., Gupta, R., Joshi, R. V., and Roodi, G. H. (2012a). "Geosynthetic-reinforced unbound base courses: quantification of the reinforcement benefits." *Rep. FHWA/TX-10/5-4829-01-1*, Center for Transportation Research, Austin, TX.
Zornberg, J. G., Mitchell, J. K., and Sitar, N. (1997). "Testing of reinforced soil slopes in a geotechnical centrifuge." *ASTM Geotech. Test. J.*, 20(4), 470–480.
Zornberg, J. G., Roodi, G. H., Ferreira, J., and Gupta, R. (2012c). "Monitoring performance of geosynthetic-reinforced and lime-treated low-volume roads under traffic loading and environmental conditions." *Proc., Geo-Congress 2012: State of the Art and Practice in Geotechnical Engineering*, ASCE, Reston, VA, 1310–1319.
Zornberg, J. G., Sitar, N., and Mitchell, J. K. (1998b). "Limit equilibrium as basis for design of geosynthetic reinforced slopes." *J. Geotech. Geoenviron. Eng.*, 10.1061/(ASCE)1090-0241(1998)124:8(684), 684–698.
Zornberg, J. G., Sitar, N., and Mitchell, J. K. (1998a). "Performance of geosynthetic reinforced slopes at failure." *J. Geotech. Geoenviron. Eng.*, 10.1061/(ASCE)1090-0241(1998)124:8(670), 670–683.